Drag Reduction Analysis of Optimal Three-dimensional Bumps on the M6 Wing

Jianfeng Gao [1, *]

[1] Shanghai Aircraft Design and Research Institute, Shanghai 201210, China.

[*] gaojianfeng@comac.cc

Abstract. Based on Isight optimization software and evolutionary strategy algorithm, this paper builds a bump optimization design platform by integrating the three-dimensional bump shape generator program, grid generation software Gridgen and flow field simulation software Fluent. This platform is successfully validated on the RAE2822 supercritical infinite straight wing, which reduces the drag coefficient by 11 counts and increases the lift-drag ratio by 11.48 percent. Through this platform, the drag reduction characteristics of optimal three-dimensional bumps on the M6 wing are numerical studied. The results show that the three-dimensional bumps can weaken shock waves and have spanwise characteristics, the stronger the shock waves, the more obvious the drag reduction effect of the three-dimensional bumps, and the wing with optimal three-dimensional bumps can improve flow field characteristics and prevent flow separations.

Keywords: Drag reduction; Shock control bump; Optimization design platform; Evolutionary strategy algorithm.

1. Introduction

The wing is the main source of aerodynamics of aircraft, and its increase in lift and drag reduction are the main goals of aircraft optimization design. Currently, civil aircrafts use supercritical wings, which can delay but not eliminate the generation of shock wave.

By far some scholars and institutions have carried out relevant research and obtained many results. In 1992 Ashill et al. [1] proposed a novel technique so–called shock control bump (SCB) to control the shock intensity of laminar flow airfoil and reduce drag; In 2008, Qin et al. [2,3] used experimental measurement and numerical simulation methods to further study the transonic flow mechanism of three-dimensional bump, which obtained the consistent results that the shock position at the working section is not only affected by the back pressure and wall effect, but also related to the boundary layer. The numerical simulation results are consistent with Baldwin–Lomax and $k-\omega$ turbulence models, and both experimental and computational methods confirm that a pair of vortices are formed in the boundary layer of the three-dimensional bump; The optimal design of two-dimensional and three-dimensional bump on natural laminar wing at transonic speeds is studied. It is pointed out that they have identical drag reduction effect at the given design condition, but in practical applications three-dimensional bump is much better; In 2023, Di Pasquale D, Prince S [4] studied the locally increased boundary layer displacement thickness can act as a virtual shock bump, and performed an experiment investigation on the flow characteristics of airfoil with sub-boundary layer scale period roughness technique through wind tunnel, the shadowgraph flow visualization showed that the bump can bifurcate the shock wave and delay shock-induced separations.

In this paper, the shock wave is passive controlled by installing a three-dimension bump on the wing. As shown in figure 1, the bump adopts the smooth concave-convex-concave form to change the normal shock wave into a series of oblique shock waves near the foot point of the shock, thereby weakening the shock wave intensity and reducing wave drag. The bump's structure is relatively simple and easy to install. It neither destroys the original structure of the wing nor requires the additional devices. In addition, the bump only optimizes the local flow field, suppresses the oscillation caused by shock wave induced separation, and has little impact on the entire flow field.

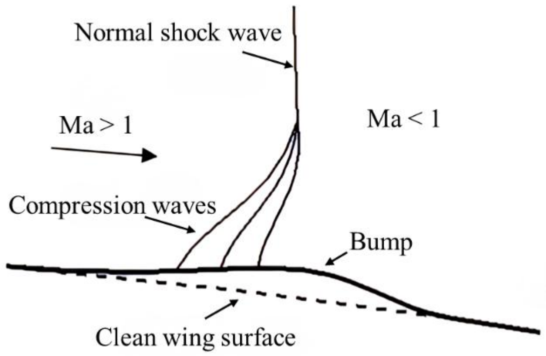

Fig. 1 Schematic diagram of shock control bump on the wing

2. Bump Optimization Design Platform

As shown in figure 2, the integrated bump optimization design platform based on Isight software consists of four modules, which are geometry module, grid generation module, flow field solution module and optimization module. Data and files are passed between them through end-to-end connection, and the optimization process is automated without manual intervention. The (1+1)-ES [5] method of evolutionary strategy algorithm is adopted as optimization algorithm, and the workflow of it is shown in figure 3. Although the form is relatively simple, it is suitable for nonlinear and discontinuous design space, and it is also very effective for dealing with problems with fewer design variables and noise. In this paper, the optimization process adopts single-objective optimization, which means the drag coefficient is minimized. The optimization iteration steps N is set to 100. The number of optimizing should no less than two times and take the optimum.

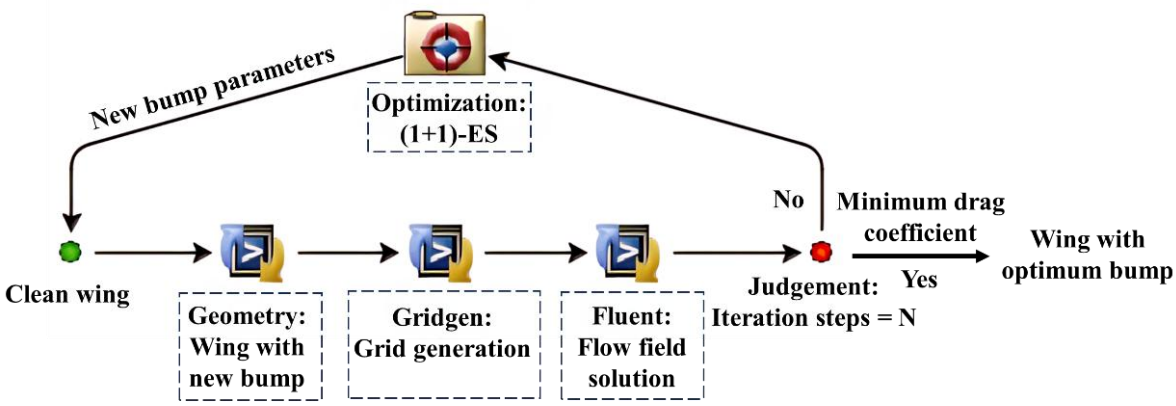

Fig. 2 Flowchart of integrated bump optimization design platform

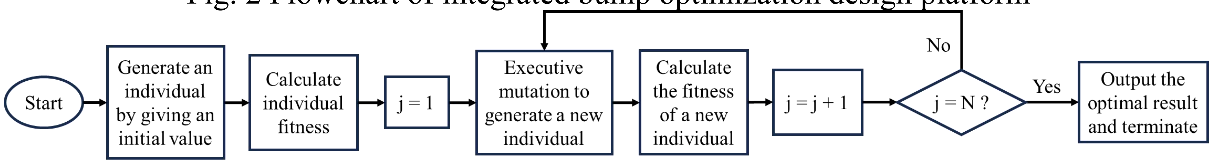

Fig. 3 Workflow of (1+1)-ES method

3. Parameterization of the Three-dimensional Bump

As is shown in figure 4, the three-dimensional bump adopts symmetrical structure. Taking half of the bump as an example, it is defined by six key variables. They are the bump length L, bump height H, the distance between the front of the bump and the leading edge of the wing Xb, the distance between the front of the bump and the bump Crest (in this paper, Cb=Crest/L is used to represent the relative crest position of the bump), and plus two spanwise parameters are bump width

Z_{width} and spacing Z_{span}. The sum of the spanwise width and spacing of the bump S is the distance of between the adjacent bumps. In order to simplify the problem, let variable S be a constant value, then the bump span parameter can only be represented by Zb ($Zb=Z_{width}/S$). The shape of three-dimensional bump is generated by the Hicks-Henne type function equation (1) [6] which controls the chord direction and the cubic polynomial equation (2) which controls the span direction. Where x is the normalized coordinate of bump in the chord direction, H_{crest} is the value of bump crest in the y direction, and z is the spanwise coordinate of the bump. The formulas are simple in form, but can generate a smooth shape. The spanwise shape of the three-dimensional bump is controlled by five curves. If the wing is a straight wing, curves 1 and 5 are straight lines. Otherwise, these two curves need to be projected onto the clean wing surface. Curves 2, 3 and 4 are generated by equation (2).

$$H = f(x) = \begin{cases} \sin^4(\pi x^m), m = \dfrac{\ln(0.5)}{\ln(Cb)}, Cb \geq 0.5 \\ \sin^4(\pi(1-x)^m), m = \dfrac{\ln(0.5)}{\ln(1-Cb)}, Cb \leq 0.5 \end{cases} \tag{1}$$

$$g(z) = H_{crest} \bullet \left(\frac{2}{Z^3_{width}} z^3 - \frac{3}{Z^2_{width}} z^2 + 1 \right) \qquad 0.2Z_{width} \leq z \leq Z_{width} \tag{2}$$

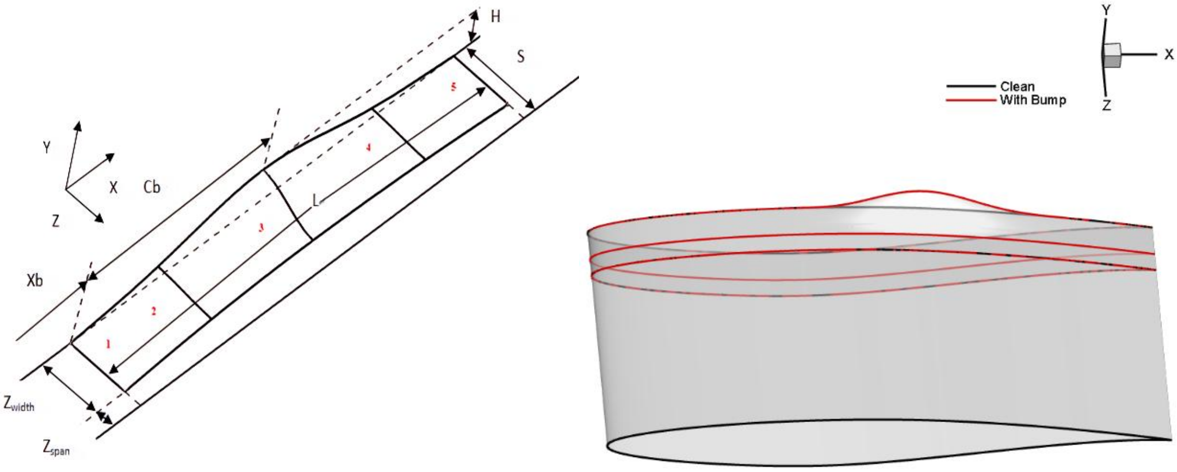

Fig. 4 Parameterization of three-dimensional bump and optimized design

4. Validation on the RAE2822 Infinite Straight Wing

In this section, the drag reduction optimization design of the RAE2822 supercritical infinite straight wing (RAE2822 wing for short) is carried out by using the bump optimization design platform. figure 5 shows the mesh of RAE2822 wing, which is O-type structured grid, and the cross sections at both ends of the wing are symmetric boundary conditions. The optimizing calculation flow conditions [7]: Ma=0.729, α=2.31°, $Re=6.5\times10^6$. RANS-equations are used in the calculation, and the turbulence model is $k-\omega$ SST model. The settings of the design variables, constraints and objective function are shown in Table 1, where the initial value of the spanwise variable Zb is set to 0.5. When Zb is 1, there is no gap between the discrete bumps, and S is 0.1 times the wing chord length.

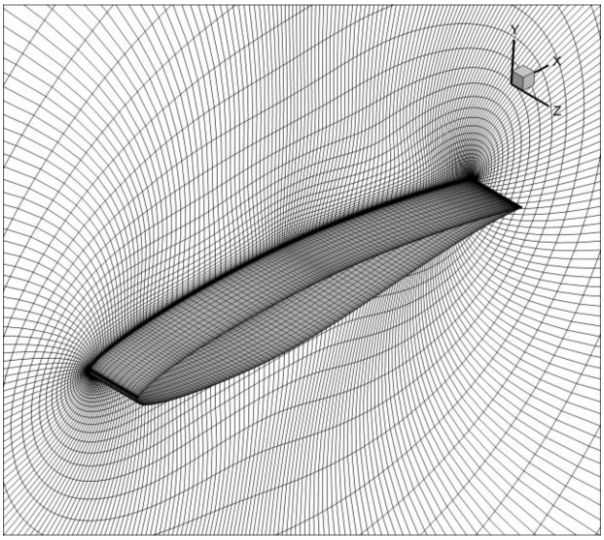

(a)clean wing

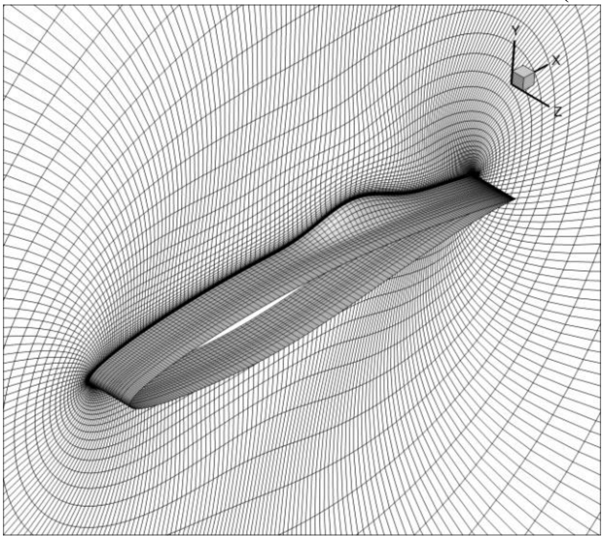

(b)wing with optimal bump

Fig. 5 Mesh of RAE2822 wing

Table 1. Settings of design variables, constraints and objective function

Symbol	Parameter	Lower bound	Upper bound	Objective
★	H	0.001	0.06	—
★	L	0.1	0.5	—
★	Cb	0.2	0.8	—
★	Xb	0.1	0.5	—
★	Zb	0.2	1.0	—
△	Cl	Cl_{clean}	—	—
△/√	Cd	—	Cd_{clean}	Minimum

The symbol "★" represents the design variable, the symbol "△" represents the constraint, the symbol "√" represents the objective function, and the symbol "—" indicates not applicable. Cl_{clean} and Cd_{clean} are the lift and drag coefficients of clean wing respectively.

The optimization results in table 2 show that the drag coefficient is reduced by 11 counts and the lift-drag ratio is increased by 11.48% when the wing is equipped with an optimal bump. Figure 6 shows the surface pressure contour and streamline distribution of the clean wing and wing with an optimal three-dimensional bump. As it can be seen, there is also no flow separation around the optimal three-dimensional bump compared to the clean wing. In order to study the spanwise flow of the three-dimensional bump, the following five sections are made in spanwise direction: $z=0, z=Z_{width}/2, z=Z_{width}, z=Z_{width}+Z_{span}/2, z=S$. Figure 7 shows the section diagram and the pressure coefficient curve of wing with optimal three-dimensional bump, reflecting the spanwise flow of bump. As the height of bump decreases, the drag reduction method of isentropic compression is still applicable, the shock wave's structure also changes accordingly, and the influence on the flow field decreases gradually. This effect not only affects the bump area, but also affects the flow of adjacent area.

Table 2. Optimization results

	H	L	Cb	Xb	Zb	Cl	Cd	ΔCd	K	ΔK
clean	—	—	—	—	—	0.7225	0.0128	—	56.45	—
optimum	0.01304	0.5	0.44	0.36	0.516	0.7363	0.0117	0.0011	62.93	11.48%

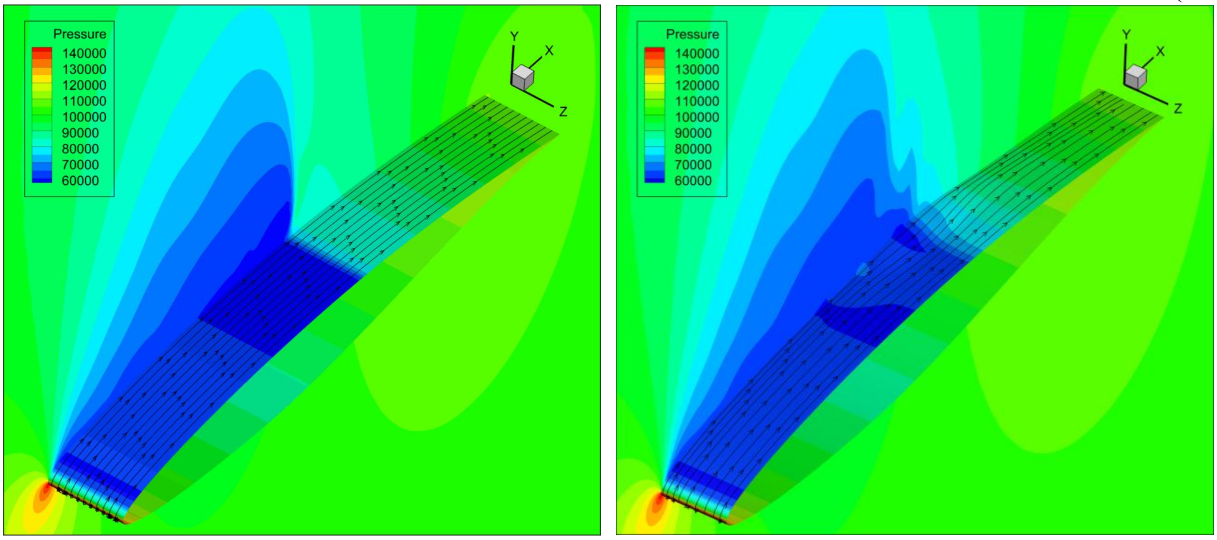

(a)clean wing (b)wing with optimal bump

Fig. 6 Surface pressure contour and streamlines of the RAE2822 wing

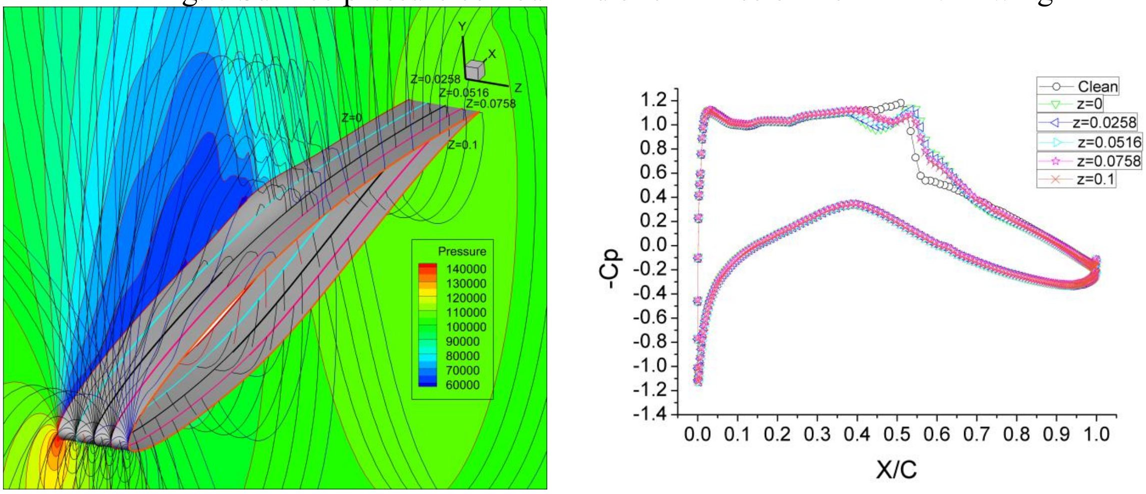

Fig. 7 Schematic diagram of wing section and pressure coefficient curve

5. Optimal Three-dimensional Bumps on the M6 Wing

The drag reduction research of the M6 wing is conducted by comparing the clean wing with wing with optimal three-dimensional bumps. The grid is C-H-type structured mesh, as shown in figure 8. Refinement is performed near the bump area, and the mesh size ranges from 0.7 to 1.77 million, which depends on the number of bumps. The optimizing calculation flow conditions [8]: Ma=0.8395, α=3.06°, Re=11.72×10^6. The profile of wing root is set as symmetric boundary. RANS-equations are used in the calculation, and the turbulence model is $k-\omega$ SST model. In order to study the spanwise flow of the three-dimensional bumps, the following five sections are made for a single bump in the spanwise: z=0(bump's symmetry plane), z=-Z_{width}, z=-S, z=Z_{width}, z=S. The settings of bump design variables, constraints and objective functions are shown in Table 3. Figure 9(a) shows the surface pressure contour and streamlines of clean wing flow field. It can be seen there are strong shock waves and flow separations in the wingtip area, and relative weak shock waves in other areas. Therefore, the entire wing is divided into 11 equal sections of 3 areas along the spanwise, and the specific plan is as follows:

1) Wing root area. This area is relatively stable, and the bump is installed at number 1 section as the optimization object, which is denoted as test1.

2) Middle wing. Strong shock waves gradually appear at the front edge of this region, but it is not suitable for placing a larger size bump. However, there are shock waves in the central part,

where can be considered to install a bump to control the shock waves. Therefore, a bump is installed at the number 7 section as the optimization object, which is denoted as test2.

3) The wingtip. This area appears strong shock waves, the flow is separated at the leading edge, which has a certain distance from the position of shock waves. This area is the critical place for arranging bumps, so optimal bumps are installed at number 9, 10 and 11 sections, which are denoted as test3, test4 and test5 respectively.

4) The above three plans are individually optimized for drag reduction. Finally, the above individually optimal bumps are combined for flow field calculation, and are denoted as test6 and test7.

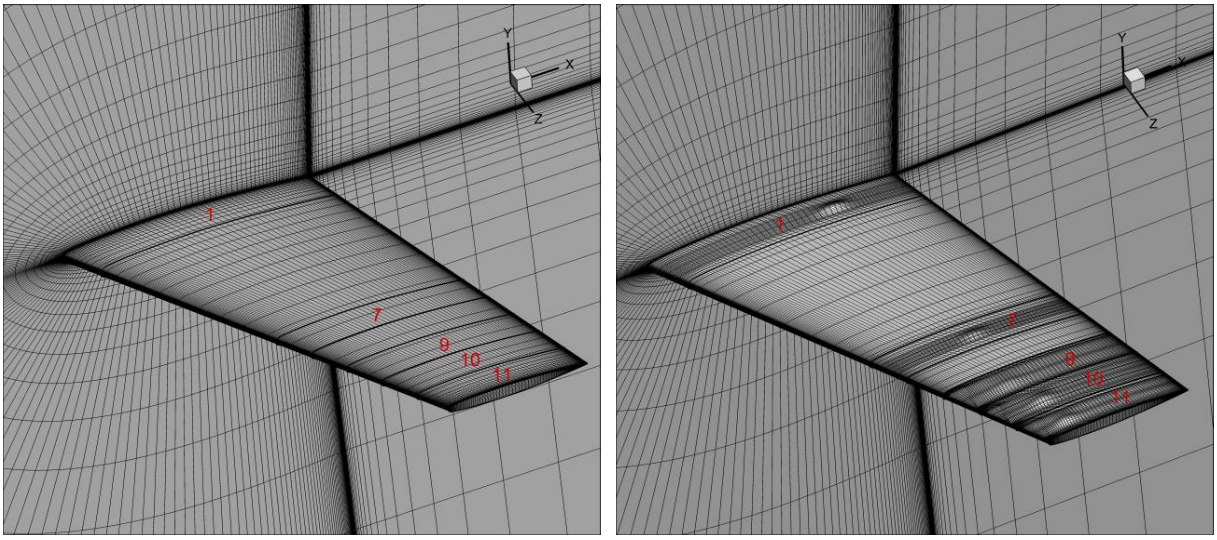

(a)Clean wing(test0) (b)Wing with Optimal bumps(test7)

Fig. 8 Mesh of M6 wing

Table 3. Settings of design variables, constraints and objective function

Symbol	Parameter	Lower bound	Upper bound	Objective
★	H	0.001	0.04	—
★	L	0.2	0.4	—
★	Cb	0.2	0.8	—
★	Xb	0.05	0.6	—
★	Zb	0.2	1.0	—
△	Cl	Cl_{clean}	—	—
△/√	Cd	—	Cd_{clean}	Minimum

Table 4. Optimization results

Plan	Section	H	L	Cb	Xb	Zb	Cd	ΔCd
test0	—	—	—	—	—	—	0.01701	—
test1	1	0.01624	0312	0.608	0.5	0.48	0.01691	0.00010
test2	7	0.0139	0.3	0.5	0.321	0.48	0.01698	0.00003
test3	9	0.01197	0.4	0.524	0.0725	0.774	0.01688	0.00013
test4	10	0.02113	0.394	0.614	0.0538	0.683	0.01670	0.00031
test5	11	0.01936	0.308	0.416	0.101	0.676	0.01680	0.00021
test6	9+10+11	/	/	/	/	/	0.01652	0.00049
test7	1+7+9+10+11	/	/	/	/	/	0.01638	0.00063

Table 4 shows the optimization results of the optimal bumps, in which symbol "+" represents the combination. Let Cd=0.0001 be a drag coefficient unit, denoted as 1 count. It can be seen from the table that all plans have good drag reduction effects. The optimal bump installed at the wing root test1 and the middle of the wing test2 reduce the drag coefficient of the wing by 1 count and 0.3 counts respectively, while the optimal bump installed at the wing tip in the strong shock wave area reduces the drag coefficient by 3.1 counts at most, indicating that the stronger the shock wave, the more obvious the drag reduction effect of the three-dimensional bump. This also reflects the correctness of the design of the bump arrangement plan for the strong shock region. However, there is also a "paradox" in the table:

1) test6 is a combination plan, and the drag coefficient decreases by 4.9 counts compared with the clean wing. If we consider a separate optimization result and simply add the drag reduction effect of test3, test4 and test5, the total amount will be 6.5 counts, which is 1.6 counts more than test6, and the drag reduction effect is better. Therefore, the drag reduction effect of bumps cannot be performed by simple addition operations.

2) test7 is also a combination plan, and the drag coefficient relative to the clean wing decreases by 6.3 counts. If a separate optimization result is considered, and the drag reduction effect of test1, test2 and test6 is simply added, the total amount will be 6.2 counts, which is basically the same as test7. Therefore, the drag reduction effect of bumps can be simply added.

In fact, there is no "paradox" in combination and simply adding the drag reduction effect of the bump. During calculation, the discrete bumps will interfere with each other and affect the flow field. When the distance between the bumps is relatively close or a bump is within the influence of the other, the interference between the bumps and the flow field will "react" and finally reach a balance. This "reaction" may have both advantages and disadvantages in the flow field, which is related to the distance between the bumps, bump's shape, etc. In this paper is adverse interference. When the bump is far apart or the bump exceeds the influence of others, the flow field between them is not affected, and the drag reduction effect can be superimposed. It can be seen from figure 9 and figure 10, the bump only affects the local flow field, improves the flow characteristics in the vicinity and prevents flow separation, and the flow around bump has a spanwise characteristic.

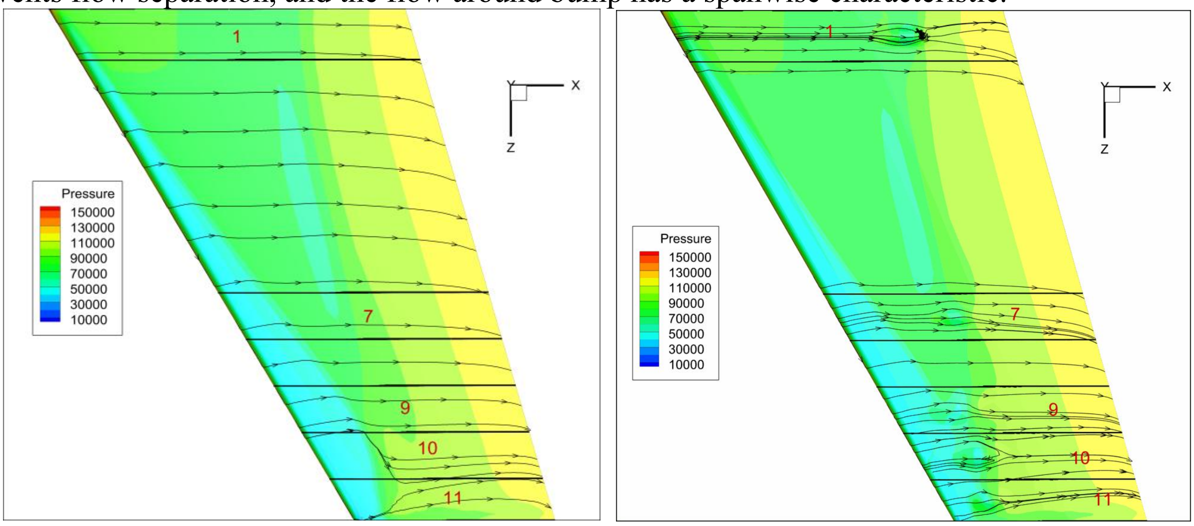

(a)test0 (b)test7

Fig. 9 Surface pressure contour and streamlines of the M6 wing

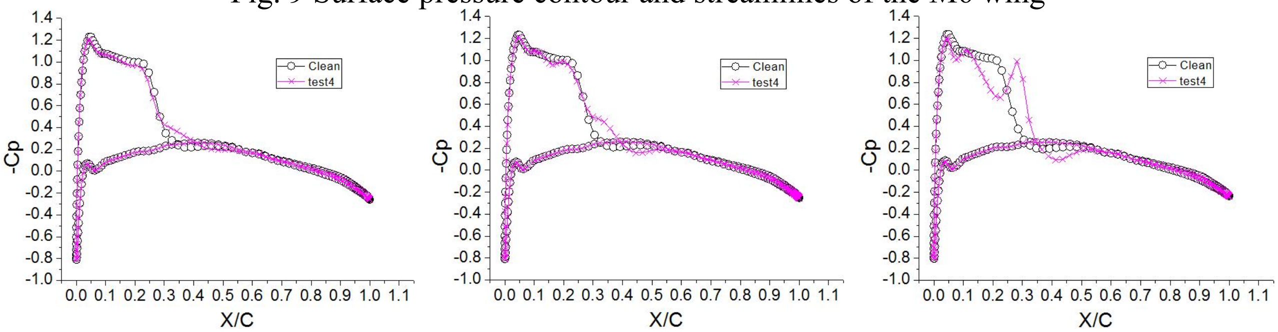

(a) z=0.9926m (b) z=1.0099m (c) z=1.0471m

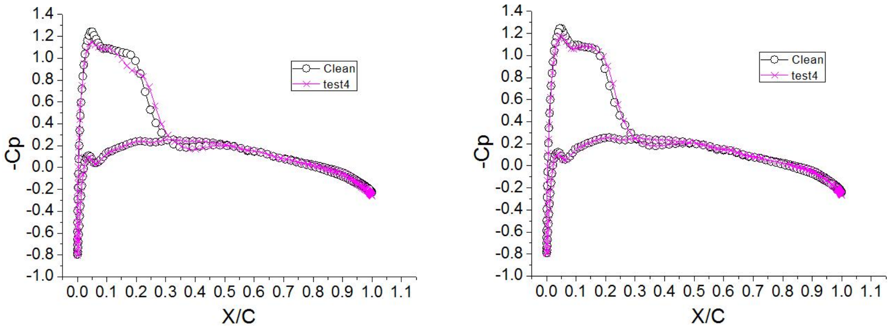

(d) z=1.0844m (e) z=1.1017m

Fig. 10 Cp distribution over the M6 wing's section of test4

6. Summary

The conclusions derived from this study are:

1) The integrated bump optimization design platform based on Isight software can automatically and efficiently generate and optimize the three-dimension bumps for the RAE2822 and M6 wings to achieve the purpose of drag reduction, indicating that the platform is feasible.

2) Since the three-dimensional bump has a spanwise structure, the flow around it also has spanwise characteristics, and the drag reduction effect will be gradually weakened with the increasing distance from the neutral surface of the bump.

3) Under certain optimization conditions, the optimal three-dimension bumps can not only improve the aerodynamic characteristics of the wing, but also improve the quality of the flow field by changing the local flow, delaying or even preventing the emergence of flow separation.

4) The stronger the shock waves, the more obvious the drag reduction effect of the three-dimensional bumps.

References

[1] Ashill P R, Fulker J L. 92-01-022 A Novel Technique for Controlling Shock Strength of Laminar-Flow Aerofoil Sections[J]. DGLR BERICHT, 1992: 175-175.

[2] Wong W S, Qin N, Sellars N, et al. A combined experimental and numerical study of flow structures over three-dimensional shock control bumps[J]. Aerospace Science and Technology, 2008, 12(6): 436-447.

[3] Qin N, Wong W S, Le Moigne A. Three-dimensional contour bumps for transonic wing drag reduction. Proceedings of the Institution of Mechanical Engineers, Part G: Journal of Aerospace Engineering, 2008, 222(5): 619-629.

[4] DI PASQUALE, Davide; PRINCE, Simon. Passive Transonic Shock Control on Bump Flow for Wing Buffet Suppression. Aerospace, 2023, 10.6: 569.

[5] Beyer H G, Schwefel H P. Evolution strategies–A comprehensive introduction[J]. Natural computing, 2002, 1(1): 3-52.

[6] Wu H Y, Yang S, Liu F, et al. Comparison of three geometric representations of airfoils for aerodynamic optimization[C]//16th AIAA Computational Fluid Dynamics Conference. 2003.

[7] COOK, P. H.; MCDONALD, M. A.; FIRMIN, M. C. P. Aerofoil RAE 2822—Pressure Distributions and Boundary Layer and Wake Measurements, AGARD AR 138, 1979.

[8] Schmitt V. Pressure Distributions on the ONERA M6-Wing at Transonic Mach Numbers, Experimental Data Base for Computer Program Assessment[J]. AGARD AR-138, 1979.